

RESEARCH ARTICLE

Siting wind turbines near cliffs – the effect of wind direction

J. Rowcroft, D. Burton, H. M. Blackburn and J. Sheridan

Department of Mechanical and Aerospace Engineering, Monash University, Clayton, Victoria 3800, Australia

ABSTRACT

The optimal siting of wind turbines in the vicinity of cliffs is investigated with respect to inflow yaw angle, using wind tunnel experiments. Wind statistics are measured above a generic forward facing step, namely, the speed-up, turbulence intensity, changes in wind direction and the persistence and frequency of vortices shed from the crest of the cliff. The experiments demonstrate that at half a cliff height above the cliff, and that same distance downstream of the crest, there exists an optimal region with increases in wind speed, combined with lower levels of turbulence intensity across the range of inflow angles that were investigated. In contrast, the far wake experiences a velocity deficit and an increase in turbulence intensity, when compared with the inflow. Furthermore, vortices are shed from the downstream reattachment region and persist beyond 10 cliff heights downstream. Copyright © 2015 John Wiley & Sons, Ltd.

KEYWORDS

forward facing step; wind direction; wind tunnel testing; wind turbine siting

Correspondence

J. Rowcroft, Department of Mechanical and Aerospace Engineering, Monash University, Clayton, Victoria 3800, Australia.

E-mail: jerome.rowcroft@monash.edu

Received 2 February 2015; Revised 18 May 2015; Accepted 31 August 2015

1. INTRODUCTION

Various wind farms across the world are sited atop sheer cliffs, particularly in coastal locations. The cubic relationship between velocity and power output provides the impetus for siting wind turbines in locations with long ocean fetches and topography-induced speed-up.^{1,2} In siting wind turbines, the wind speed is one of the primary variables determining the financial viability of a wind farm.² However, turbulence intensity (TI), variation in wind direction, inflow angles and low-frequency buffeting from persistent vortices shed from the crest of the cliff affect wind turbine fatigue loading, wind-rotor alignment and power output.

Previous studies have investigated cliffs by using the forward facing step (FFS) as a first-pass approximation. These investigations have characterized the speed-up, TI, flow separation, size of the recirculation region, effects of boundary layer thickness and Reynolds number over FFSs, as well as having described the underlying flow structure and aspects of the flow dynamics.^{1,3–9} Nevertheless, the effect of wind direction on the flow over an FFS has been given little attention, yet variations in wind direction as a function of spatial location remain an important consideration in wind turbine siting.

A schematic of the flow structure and the inflow and geometric parameters associated with the FFS are shown in Figures 1 and 2. In siting wind turbines on cliffs, the aim is to capture the maximum wind speeds induced by the FFS, whilst avoiding the regions associated with the flapping vortices shed from the crest of the FFS. Researchers such as Sherry *et al.*,⁹ Castro and Dianat³ and Largeau and Moriniere⁵ warn of the recirculation region immediately downstream of FFSs, the size of which is typically measured using the mean reattachment length, X_L , as a proxy.

In particular, a work by Kiya and Sasaki⁴ was able to characterize the structure of the recirculation region downstream of a sharp-edged, blunt flat plate. Measurements along the edge of the shear layer revealed a linear increase of the integral time scales, increasing as a function of distance downstream. From this observation, they deduced that the rolled-up vortices from the sharp edge successively amalgamate upstream of the reattachment. They characterized regular shedding of 'large-scale' vortices from this recirculation region. They also observed the accumulation of vorticity in that region, resulting in the growth of the recirculation region, followed by the ejection of an 'extremely large' vortex and a

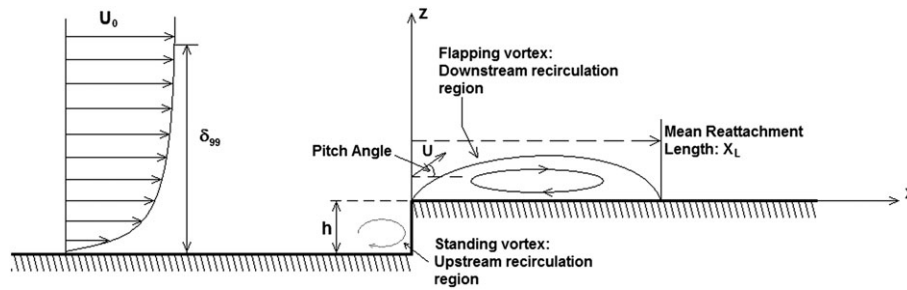


Figure 1. Diagram of forward facing step.

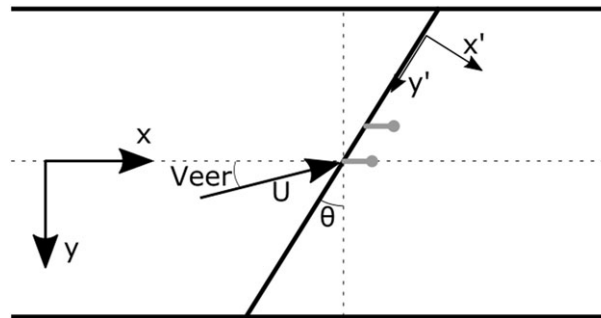


Figure 2. Plan view illustrating orientation of the co-ordinate systems. The orientations of the probes are shown in grey. The heads are facing in the $-x$ direction, but aligned laterally, parallel to the crest in the y' direction.

corresponding reduction in size of the recirculation region. The ejection of this larger-scale vortex was observed at one-sixth the frequency of the standard large-scale vortex ejection.

The persistence of these flow structures downstream will adversely affect wind turbines that are sited downstream of the mean reattachment region, as they will be subjected to the buffeting associated with the turbulent recirculation region, and resulting vortex ejections cause a reduction of both instantaneous energy production and increased fatigue loading. Pitch angles, regions of high shear and veer (change of wind direction with height) all impart unbalanced loads across the wind turbine rotor.

An important parameter affecting the size and behaviour of the separation bubble is the ratio of boundary layer thickness to step height (δ/h). Largeau and Moriniere⁵ highlight that the size of the downstream recirculation region increases as δ/h is reduced because the inflow TI, which is largest near the surface, will interact with the separation region, facilitating its breakdown.

The TI itself is another important parameter affecting the breakdown of the separation bubble. Hillier and Cherry,¹⁰ Kiya and Sasaki¹¹ and Saathoff and Melbourne¹² provided initial investigations into the effect of inflow TI on the separation bubble on a flat plate. Kiya and Sasaki¹¹ controlled TI by placing a thin rod ahead of the flat plate, with the TI controlled by varying the diameter of the rod and the distance of the rod from the plate. Their results quantified the reattachment length, which they normalized against the half-thickness of the blunt, flat plate. As the TI was increased from 1% to 7%, the normalized reattachment length decreased from 10 to 3.

Field data characterizing the separation bubble, its development and dissipation are limited. Mann *et al.*¹³ used a light detecting and ranging unit to perform measurements over the 12 m high cliff on the Bolund Hill, Denmark. Wind turbine under-performance at the Tappi Wind Park, in Japan, motivated Ishihara¹⁴ to compare linear flow models with nonlinear flow models and wind tunnel models. The investigation demonstrated that flow separation from the crest of the 150 m high coastal cliffs contributed to the wind turbine under-performance.

A recent study by Rowcroft *et al.*¹⁵ tested the hypothesis that only the flow perpendicular to the crest of an FFS is accelerated, a hypothesis that Baker¹⁶ had applied to railway embankments with some success. Their work relied heavily on the conclusion from Sherry *et al.*,⁹ who established a critical Reynolds number above which X_L is largely insensitive. Rowcroft *et al.*¹⁵ supposed that if the Reynolds number of the flow component perpendicular to the crest was maintained above the critical Reynolds number, the size of the downstream recirculation region would remain constant with changes in wind direction. In their wind tunnel testing, they used surface visualization to measure X_L in a range of turbulence conditions and for various values of δ/h for yaw angles between 0° and 50° , at Reynolds numbers ranging from 1×10^5 to 3×10^5 , based on the cliff height and the free-stream velocity. In the low TI cases, where stream-wise TI was 4.6% at

the height of the FFS, increasing the yaw angle up to 40° resulted in notable increases in X_L . X_L/h increased from 2.8, at $\theta=0^\circ$, to 3.8, at $\theta=40^\circ$. They theorized that the yaw angle increased the stability of the separation region. However, in the high TI cases, where stream-wise TI was 12.3% at the height of the FFS, X_L was reduced, but the relationship between X_L and θ was less clear, with no consistent trend observed.

In the low TI cases investigated by Rowcroft *et al.*,¹⁵ the flow topology was considered using paint droplet surface shear stress visualizations. Three-dimensionality was observed in the visualizations. Such observations are expected in instantaneous measurements;⁵ the presence of lateral periodicity in the form of distinct shedding from the downstream recirculation region captured in the time-averaged surface shear stress visualizations is noteworthy.

Whilst the previous research by Rowcroft *et al.*¹⁵ extrapolated surface measurements to test their hypothesis, the current research focusses on velocity measurements collected above the FFS through various wind directions, for a single δ/h and TI profile. A quantitative assessment of Baker's proposition, which Rowcroft *et al.*¹⁵ initially measured with the proxy of X_L , is made using direct comparisons of flow velocity. Probe measurements above the surface of the FFS provide additional insight into the flow structure as it interacts with the FFS. Furthermore, the speed-up, change in TI, wind veer, pitch angle and the propagation downstream of coherent structures, which are presented, provide insight into wind turbine siting strategies.

2. METHODOLOGY

The research was conducted in the Monash University 450 kW wind tunnel, details of which can be found in Rowcroft *et al.*¹⁵ The wind tunnel is a closed-circuit wind tunnel with a 2×2 m working section of length 12 m. Upstream, a 4×3 m settling chamber containing a mesh screen is linked to the working section through a 3:1 contraction of length 2.5 m. The mesh was constructed from 0.5 mm diameter vertical and transverse elements, spaced at 2 mm intervals. The experiments were completed at Reynolds numbers of 1×10^5 , using the step height, $h = 0.050$ m, as the reference length. End plates extending $12h$ upstream of the crest and vertically $12h$ above the false floor were used. The FFS models resulted in 2.5% blockage. The yaw angles investigated were 0° , 20° , 30° and 40° . The models spanned beyond $48h$ downstream of the crest and can be thus considered isolated cliffs, exceeding the threshold of $10h$ prescribed by Moss and Baker⁷ for defining an isolated cliff at 0° yaw. The false floor extended $47h$ upstream of the centre of the crest. The aspect ratio at $\theta=0^\circ$, defined as the ratio of model width to model height, was 34. Following the work of de Brederode and Bradshaw,¹⁷ the aspect ratio ought to be maintained above 10 so that the 0° geometry can be considered two-dimensional. The finite nature of the closed jet wind tunnel implies that even at the elevated aspect ratio of 34, edge effects will be significant for non-zero yaw cases, and the lateral flow speed will tend to reduce. Paint droplet surface shear stress visualizations performed by Rowcroft *et al.* over FFSs at a range of yaw angles demonstrated that edge effects impacted significant portions of the flow.¹⁸ However, a central region, free from edge-effects, was observed for yaw angles up to 50° .¹⁸

3. INFLOW CONDITIONS

A single inflow case was examined, corresponding to the 'Low TI 2' case in Rowcroft *et al.*¹⁵ The inflow conditions were measured using a TFI four-hole pressure probe, with a 45° cone of acceptance. For the boundary layer traverse, each point was sampled for 20 s at a sampling frequency of 2500 Hz.

This wind tunnel configuration used a false floor of height 435 mm with a tapered leading edge. This configuration was used to minimize inflow turbulence, so that the flow structures would be most easily visible. Whilst the TI levels are not representative of the atmospheric boundary layer, field testing has shown that flow structures such as those associated with separation regions persist in field measurements where TI levels are much higher.^{13,14} Only the upstream mesh screen was used to condition the flow. Velocity, TI and integral length scale profiles are presented in Figure 3. TI at the top of the boundary layer was 2.5%, whilst in the free stream, it was stable below 1%. The integral length scale, approximated by fitting the von Kármán curve to the power spectral density of the stream-wise velocity time series,¹⁹ increased from 0.1 m near the surface to 0.3 m at the top of the boundary layer, before decreasing beyond the top of the boundary layer back to 0.1 m.

Lateral profiles were measured at a height of $\delta/2$; across a 0.500 m span, TI and velocity measurements yielded a lateral inflow variation envelope of less than $\pm 3.5\%$.

4. PROBE MEASUREMENTS

To measure flow statistics over the FFS geometries, the region downstream of the crest of the $h=0.050$ m FFS was traversed with two TFI four-hole pressure probes.

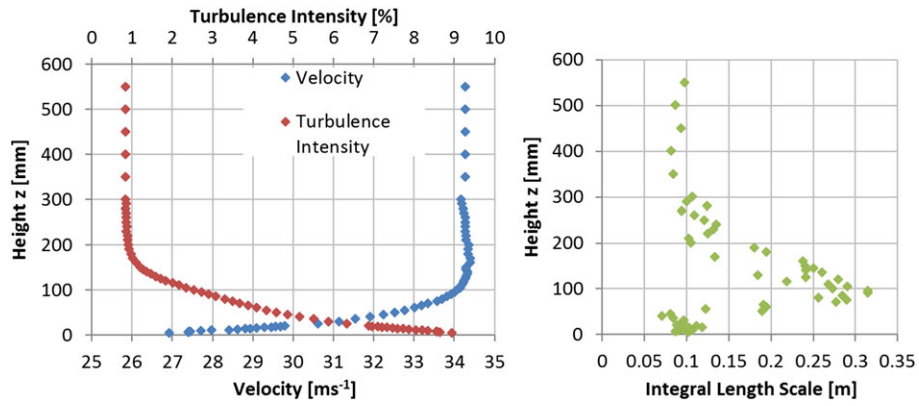


Figure 3. Inflow conditions: velocity, stream-wise TI, and stream-wise integral length scale ($\bar{x}L_{ij}$).

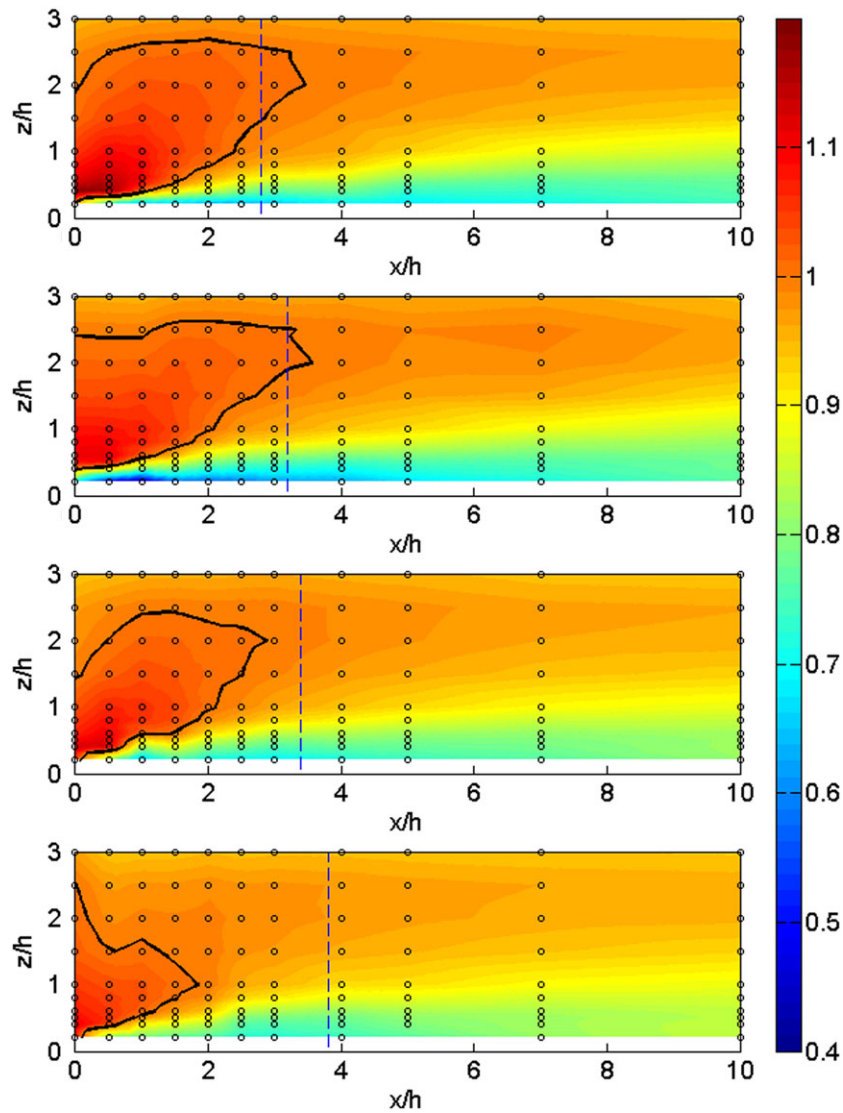


Figure 4. Map of speed-up downstream of crest of FFS, as defined by Equation E1. From top to bottom, yaw angles are 0°, 20°, 30° and 40°. Black circles represent measurement locations. Solid trace represents $S = 1$ contour. Dashed line is the mean reattachment line.

The design of the probes is presented in the work of Musgrove and Hooper.^{20,21} They consider the pressure signals from the four holes of the Cobra Probe, generating ratios between each of the pressure signals. These ratios are then related back to calibration surfaces to determine the three velocity components and the static pressure.

Various investigations have been conducted to establish the accuracy of the Cobra Probes, considering both their static response and their dynamic response. Hooper and Musgrove²⁰ showed that they are insensitive to Reynolds number for the velocity range $16\text{--}110\text{ ms}^{-1}$, giving confidence in the mean data over a broad velocity range, below speeds where measurements would be sensitive to compressibility. Hooper and Musgrove provided further dynamic validation of the Cobra Probe performance in a swirling jet²² and validated their results against hot wire anemometers and laser Doppler anemometers in fully developed pipe flow.²¹ These results demonstrated excellent frequency response up to 1500 Hz and are thus capable of resolving Strouhal numbers up to 1.125, based on the step height used in this work. The work of Largeau and Moriniere⁵ suggested that the shedding of large-scale structures would occur at Strouhal numbers as high as 0.6, whilst Camussi *et al.*²³ observed peak Strouhal numbers of 0.2 in their FFS investigations. Thus, Cobra Probes are suitable for capturing the dominant flow physics in non-reversed flow conditions.

The traverses were conducted at a sampling frequency of 5000 Hz and down-sampled to 2500 Hz over a period of 180 s.

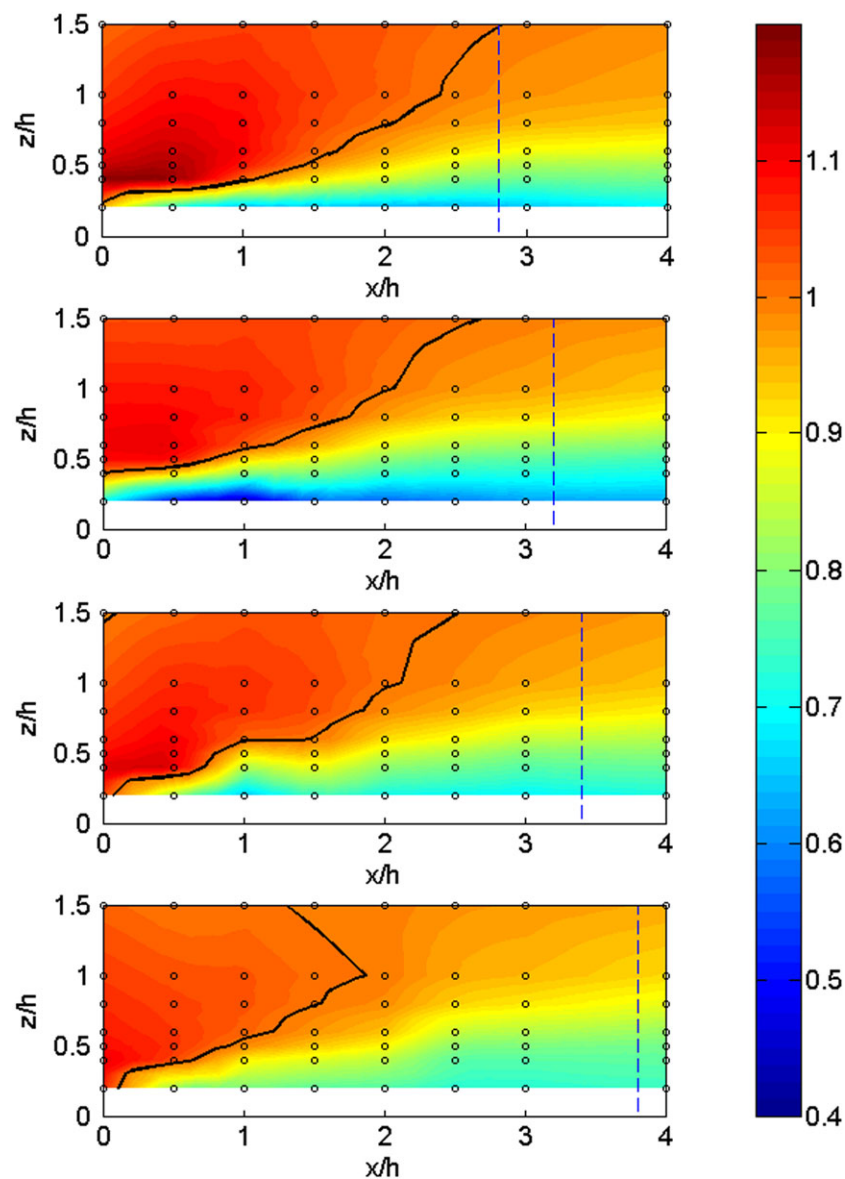


Figure 5. Magnification of speed-up in the region immediately downstream of the crest, from $0 < x < 4 h$ and $0 < z < 1.5 h$.

Free-stream velocity measurements were calculated based on dynamic pressure measurements from the up-stream Pitot-Static tube. Air density was calculated based on atmospheric pressure measured in the laboratory with a *Tief Hoch* barometer, and temperature was measured in the tunnel using a thermocouple. As shown in Figure 2, two sets of Cartesian co-ordinate systems are used. The global co-ordinate system relates to the orientation of the wind tunnel: x is the direction of the freestream flow, y is the direction perpendicular to the freestream flow, parallel to the ground plane, and z is the vertical direction. The magnitude of the wind speed is denoted by U , whilst the velocity fluctuations from the mean in the x , y and z directions are u , v and w , respectively. The local co-ordinates are based on the orientation of the FFS: x' is the direction perpendicular to the crest of the FFS, y' is the lateral direction along the crest of the FFS and z' is the vertical direction, the same orientation as z .

The probes were spaced 50 mm apart in the y' direction, and their heads were aligned parallel to the crest of the FFS, whilst facing in the $-x$ direction. The orientation and spacing of the probes are shown in Figure 2. Thus, an accurate measure of the flow within the recirculation region cannot be achieved because of the high percentage of the flow not coming from within the 45° cone of acceptance. However, in regions more advantageous to wind turbine siting, such as above and downstream of the recirculation region, reliable flow statistics have been captured.

5. DEVELOPMENT OF VELOCITY PARAMETERS AS A FUNCTION OF YAW ANGLE

The results of the pressure probe measurements are presented in the following series of figures, mapping mean speed-up, turbulence intensity ratio, pitch, yaw, cross-correlation and Strouhal number statistics for four yaw angles: 0° , 20° , 30° and 40° .

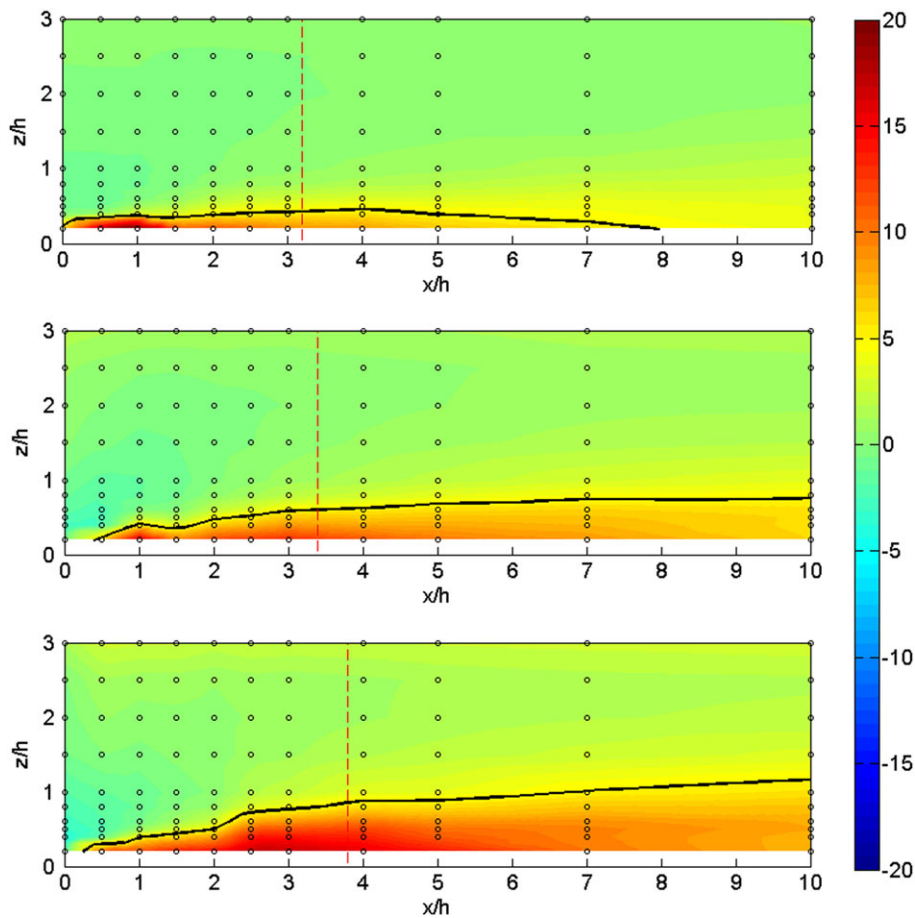


Figure 6. Comparison of experimentally measured speed-up with Baker's hypothesis. Variation between the two is expressed as a percentage, as describe in Equation E3. Model over-prediction is positive; model under-prediction is negative. Black circles represent measurement locations. Solid trace represents 5% variation contour. From top to bottom, yaw angles are 20° , 30° and 40° . Dashed line is the mean reattachment line.

Speed-up, S , is defined as follows:

$$S = \frac{U(x',z')/U_P}{U_{BL}(x=0,z)/U_{P,BL}} \tag{E1}$$

Speed-up is visualized in Figure 4, and a close-up of the crest region is shown in Figure 5. $U(x',z')$ is the magnitude of the velocity vector at a point (x',z') , according to the previously defined Cartesian co-ordinate system. U_P is the magnitude of the velocity vector measured at the up-stream Pitot-Static tube, measured concurrently to $U(x',z')$. The Pitot-Static tube was located greater than $55h$ upstream of the centre of the crest of the FFS, 12.3 boundary layer heights above the surface of the false floor. $U_{BL}(x=0,z)$ is the magnitude of the velocity vector in the undisturbed boundary layer, that is, without the model in place, at $x=0$. $U_{P,BL}$ is the magnitude of the velocity vector measured at the up-stream Pitot-Static tube, measured concurrently to $U_{BL}(x=0,z)$.

Maximum speed-up in each of the cases occurs between the crest and $2h$ downstream and above $0.5h$ from the surface of the FFS, decreasing gradually with height. As the yaw angle increases, the maximum speed-up is decreased, and the region where the speed-up is greater than one is also decreased. This is illustrated by the $S=1$ contours presented in Figure 4.

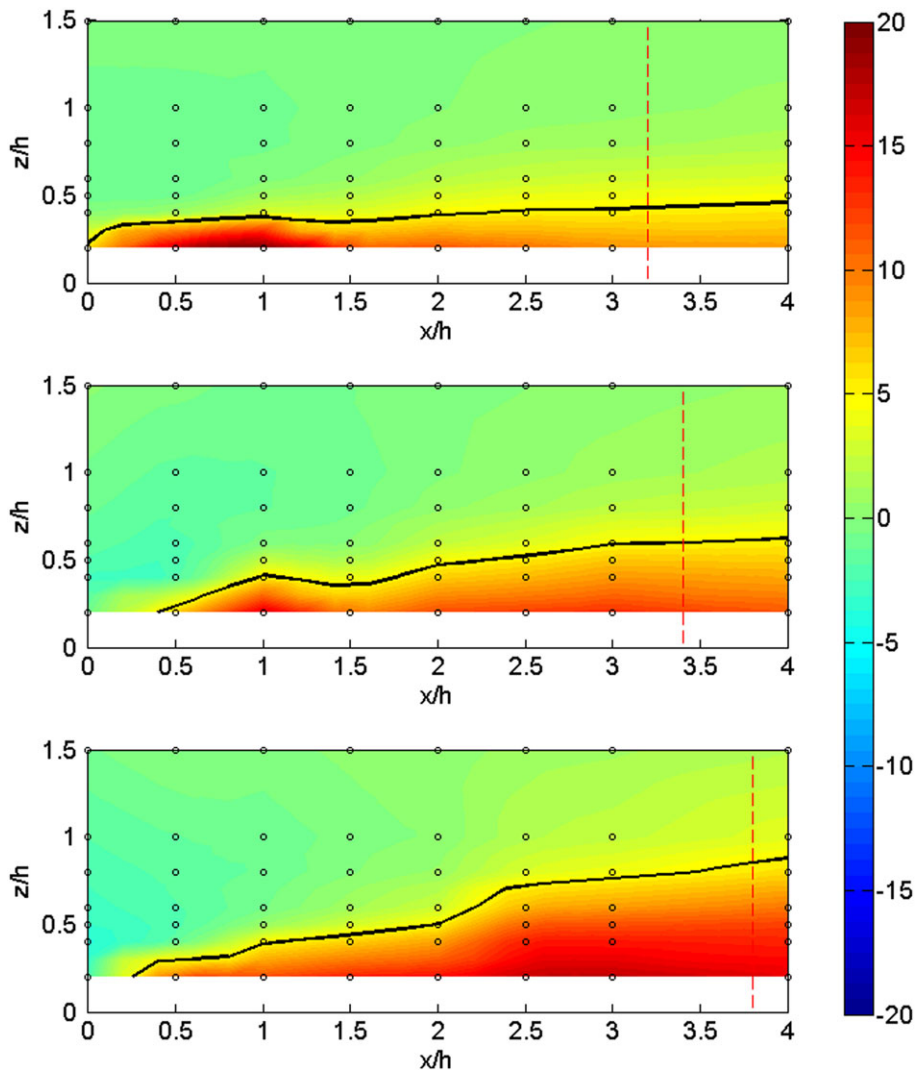


Figure 7. Magnification of comparison of experimentally measured speed-up with speed-up predicted using Baker’s hypothesis in the region immediately downstream of the crest, from $0 < x < 4h$ and $0 < z < 1.5h$.

Baker’s hypothesis is that only the component of the flow perpendicular to the FFS is accelerated. Thus, a comparison can be made with estimates based on the $\theta=0^\circ$ case with the actual speed-up measured at $\theta=20^\circ, 30^\circ$ and 40° . The predicted speed-up, S_{Pr} , based on Baker¹⁶ and Lubitz and White,²⁴ is shown as follows:

$$S_{Pr}(\theta) = \sqrt{S_0^2 \cos^2(\theta) + \sin^2(\theta)} \tag{E2}$$

In this equation, S_0 is the speed-up at $\theta=0^\circ$. The deviation of the model from the measured values is expressed as a percentage in the colour plots in Figure 6, and a close-up of the crest region is shown in Figure 7, according to the following equation:

$$\text{Variation} = \frac{S_{Pr}(\theta) - S(\theta)}{S(\theta)} \times 100\% \tag{E3}$$

The discrepancy between the predicted speed-up and the experimental measurements occurs predominantly in the recirculation region and the shedding downstream of the recirculation region. These regions are associated with the

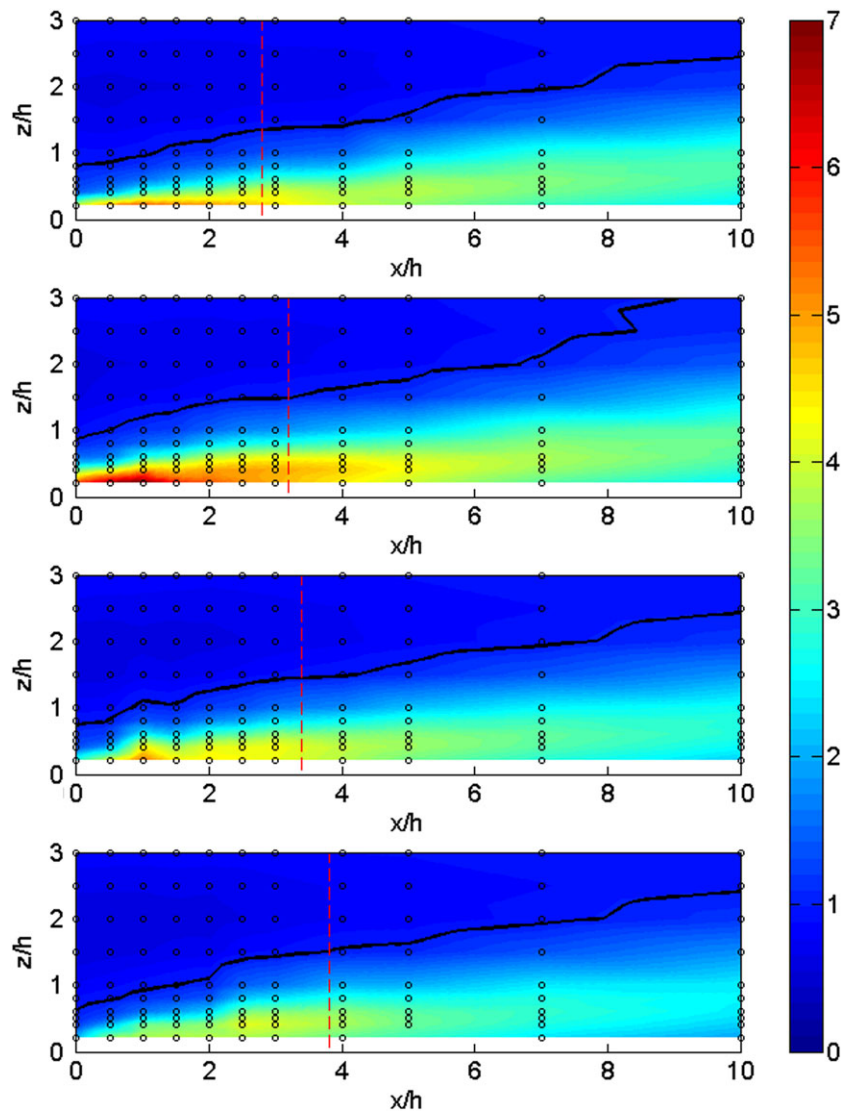


Figure 8. Map of *TI Ratio* downstream of crest of FFS, as defined by Equation E4. From top to bottom, yaw angles are $0^\circ, 20^\circ, 30^\circ$ and 40° . Black circles represent measurement locations. Solid trace represents *TI Ratio* = 1 contour. Dashed line is the mean reattachment line.

well-documented problem of pressure probe measurements being subjected to reversed flow. As the yaw angle is increased, the downstream region of over-prediction increases in size; in particular, the region of increased variation widens in the vertical dimension. The contour representing 5% variation between predicted data and experimental data is shown in each panel of Figure 6. In the $\theta=20^\circ$ case, the contour begins to decay at $x/h=4$, and never reaches above $0.5h$ above the surface. At $\theta=20^\circ$, the region where the model and the experimental data differ by greater than 5% does not appear to reduce in size with distance downstream. By $\theta=40^\circ$, the 5% contour continues to gain height through the farthest downstream measurement plane at $x/h=10$.

Thus, as yaw angle is increased, the margin between experimental data and predicted speed-up based on Baker’s hypothesis increases. However, the key area of interest is the bubble-like region where the greatest speed-up occurs. This area, which grows above the recirculation region to $1.5h$ downstream in each case, remains in excellent agreement between the experimental measurements and the predicted values, with less than 5% difference between them.

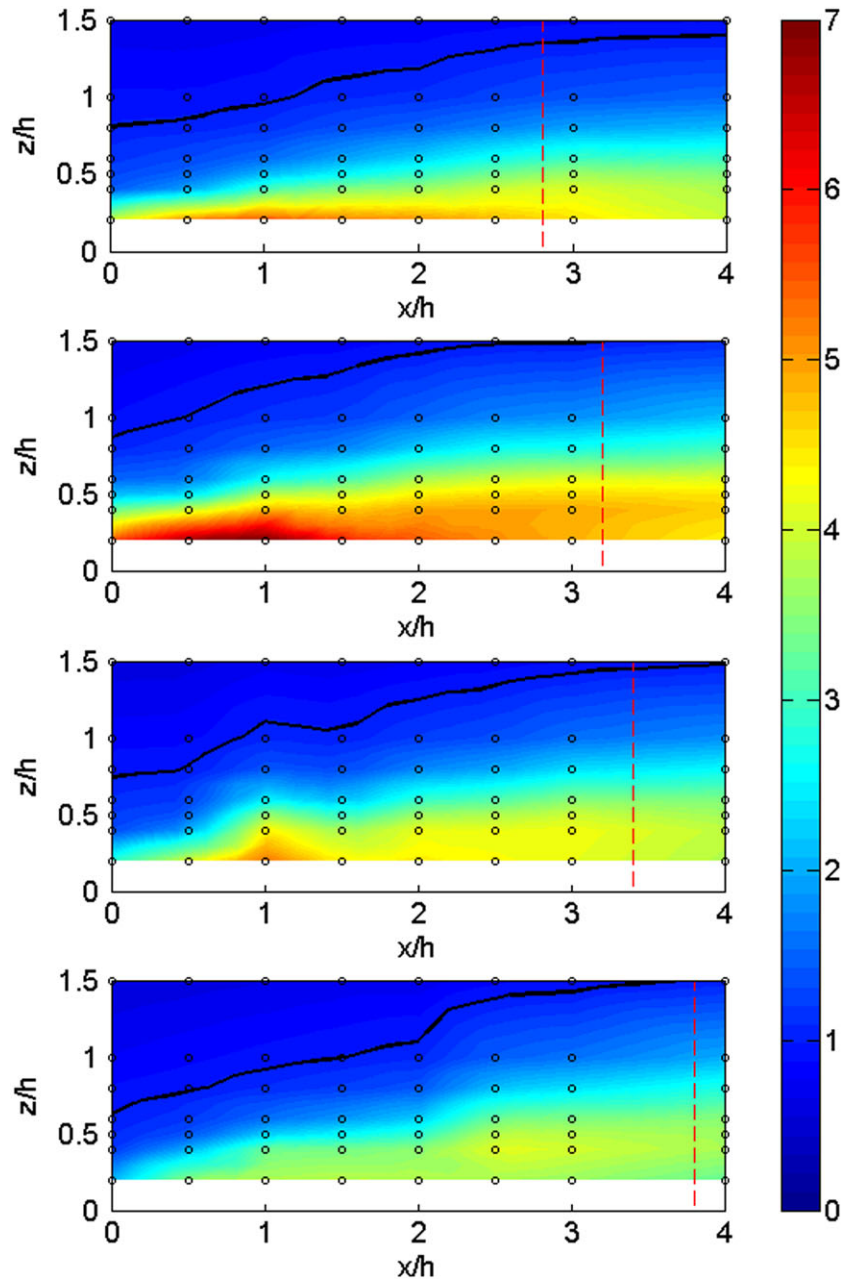


Figure 9. Magnification of *TI Ratio* in the region immediately downstream of the crest, from $0 < x < 4h$ and $0 < z < 1.5h$.

Similar to S , the change in TI, visualized in Figure 8, is expressed as a *TI Ratio* and defined according to the following equation:

$$\text{TI Ratio} = \frac{I_{uvw}(x', z')}{I_{uvw, BL}(x = 0, z)} \quad (\text{E4})$$

$I_{uvw}(x', z')$ is the TI based on the three velocity components and is defined in Equation E5.

$$I_{uvw} = \frac{\sqrt{\frac{1}{3}(\overline{u^2} + \overline{v^2} + \overline{w^2})}}{U} \quad (\text{E5})$$

The BL subscript and the (x', z') location have the same meaning as in Equation E1. A magnified version of Figure 8 in the region of the crest is presented in Figure 9.

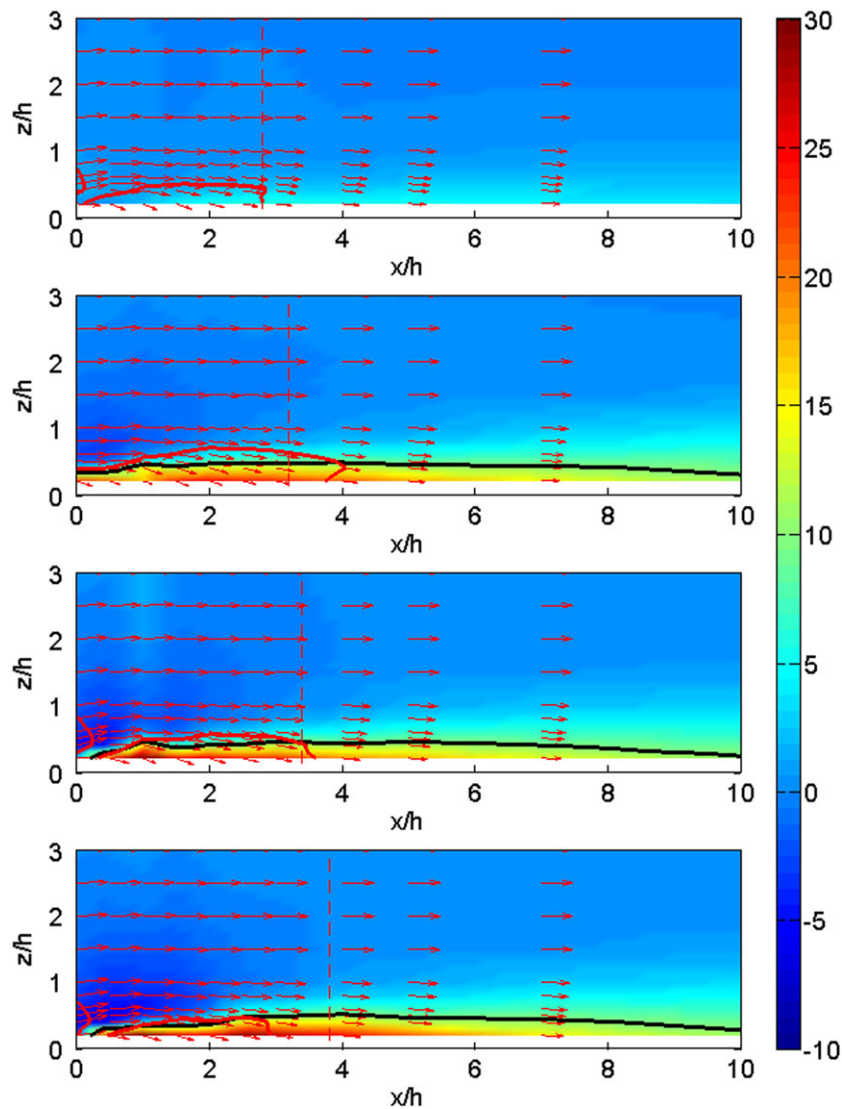


Figure 10. Map of flow veer angles downstream of crest of FFS, superimposed with velocity vector plot of pitch angles. From top to bottom, yaw angles are 0°, 20°, 30° and 40°. Black trace represents veer angle = 10° contour. Lighter coloured trace represents pitch angle = 8° contour. Dashed line is the mean reattachment line.

The region of highest TI, as shown in Figures 8 and 9, is the recirculation zone for all yaw angles examined. Beyond the recirculation region, vortices are still ejected downstream. These vortices gradually weaken, resulting in a reduction of the TI ratio. However, the TI, even $10h$ downstream, is in the order of two to three times that measured in the inflow conditions up to a height of $1.5h$ above the surface.

Wind veer, depicted in Figure 2, is defined as the angle projected on the x - y plane between the x direction and the x - y components of the local flow velocity vector. Variation in wind veer as a function of height above the surface results in yaw misalignment and imbalanced loads on wind turbine rotors. Wind veer is plotted in the colour plots in Figure 10, superimposed with a velocity vector plot showing the pitch angles. Contours representing a pitch angle of 8° are traced in lighter coloured, whilst contours representing yaw angles in excess of 10° are traced in black. A zoomed in visualization is presented in Figure 11. Ideally, wind turbines should not be subjected to large pitch angles, or variations in yaw angle as a function of height above the ground. The primary standard used in the wind energy industry to certify wind turbines is from the International Electro-technical Commission (IEC), IEC61400-1,²⁵ which requires that wind turbines be capable of operating for inflows with pitch angle up to $\pm 8^\circ$. At the crest and through the recirculation region, the pitch falls outside

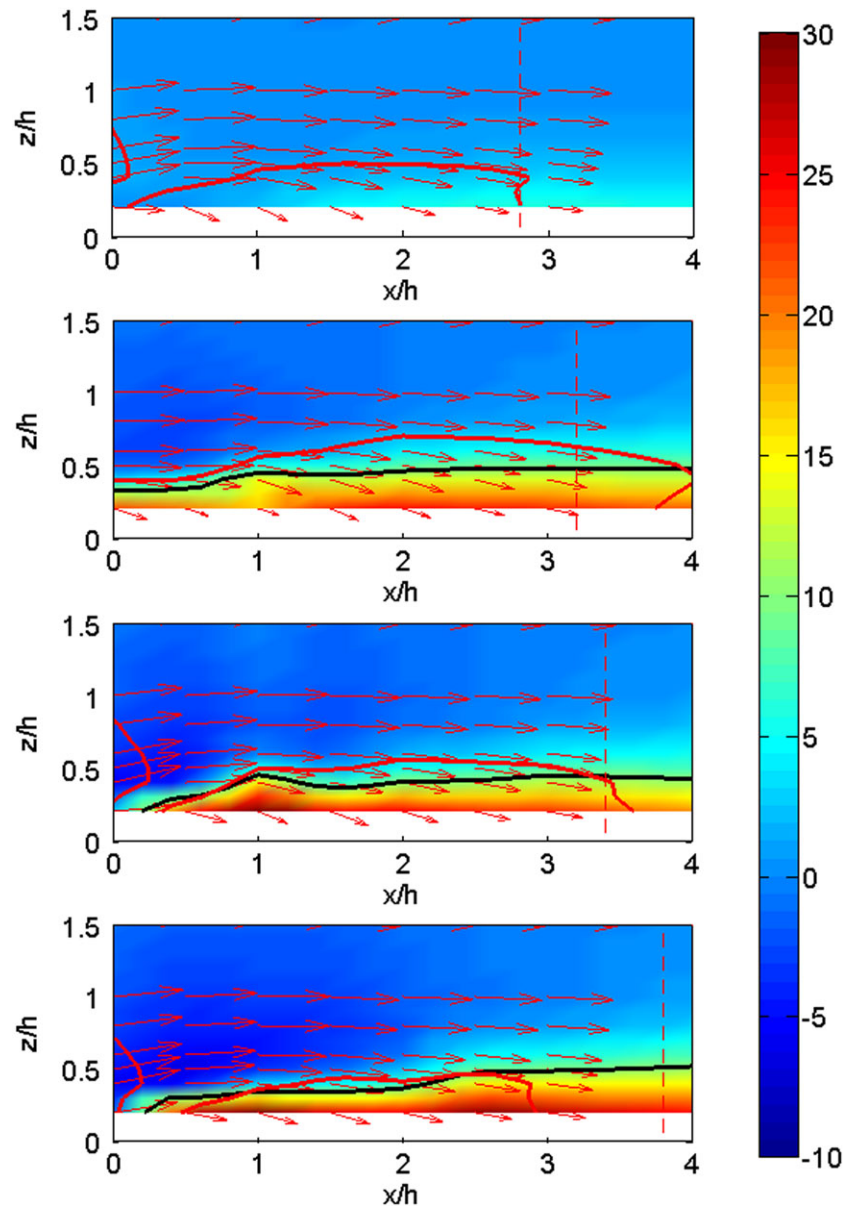


Figure 11. Magnification of pitch and veer in the region immediately downstream of the crest, from $0 < x < 4h$ and $0 < z < 1.5h$.

of this design envelope in each model. However, in each case, the measurements taken at $0.5h$ downstream of the crest, for $z > 0.5h$, were within the range of 0° – 4° .

As previously discussed, in the non-zero yaw angle cases, the veer angle will tend to be underreported because of the constrained nature of the flow. This has been mitigated by implementing an aspect ratio of 34, which is significantly larger than the minimum aspect ratio of 10, as recommended by de Brederode and Bradshaw for the 0° case.¹⁷ Surface visualizations presented by Rowcroft *et al.*¹⁵ demonstrated significant edge effects; however, a central region apparently unaffected by edge effects was also observed. Thus, measurements in this region provide an acceptable representation of the infinite step.

The measured veer angle and its variation with height above the surface prove to be an issue through the recirculation region, where speed-up is low, turbulence intensity is high and pitch angle is high. In the wake region beyond the recirculation bubble, the veer remains significant, in spite of the constrained nature of the flow. The region up to $0.5h$ above the surface undergoes a veer of greater than 10° , which can be seen in the 20° , 30° and 40° models.

Figure 12 presents cross-covariance maxima normalized by the number of samples from the two traversing Cobra Probes. A magnified view of the crest region is presented in Figure 13. The probes are spaced in the y' direction at one step height, that is, 50 mm. Within the recirculation region, near the crest of the FFS, there is clearly an increased correlation

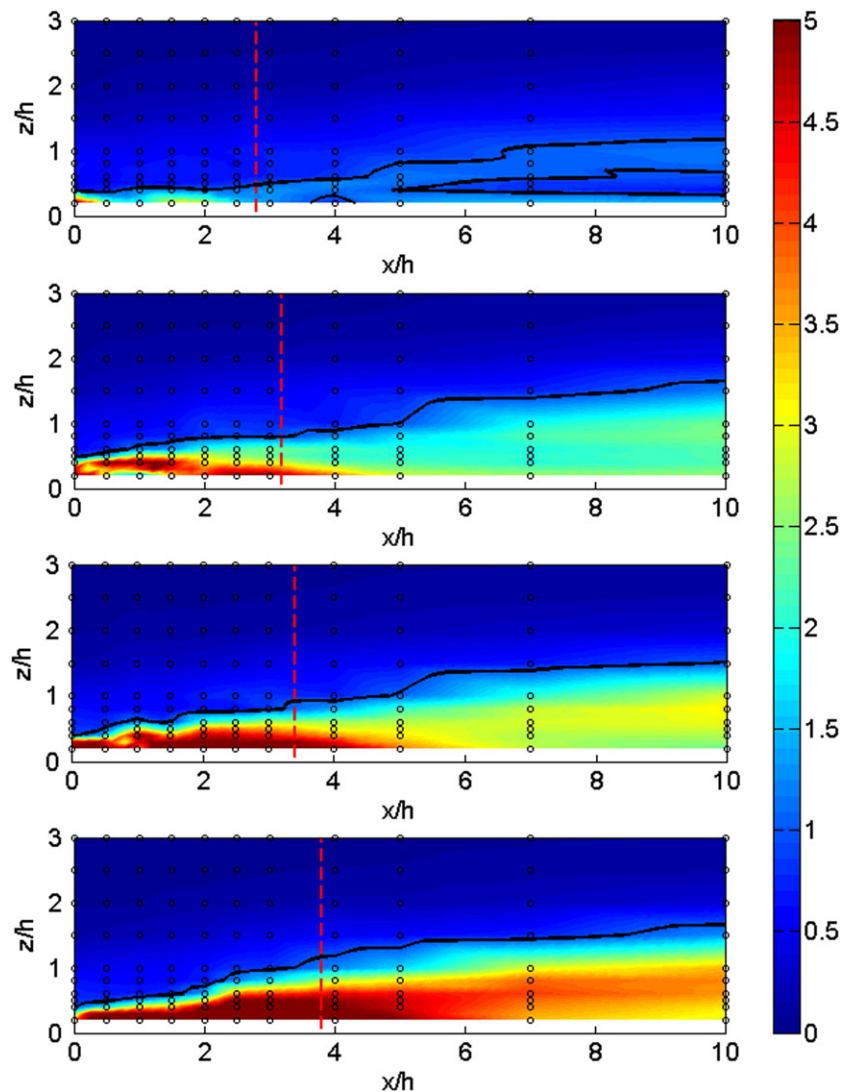


Figure 12. Plot of the normalized cross-covariances between two probes traversing $h = 50$ mm apart in the y direction over an FFS. From top to bottom, yaw angles are 0° , 20° , 30° and 40° . Black circles represent measurement locations. Dashed line is the mean reattachment line. Solid trace represents the cross-covariance = 1 contour.

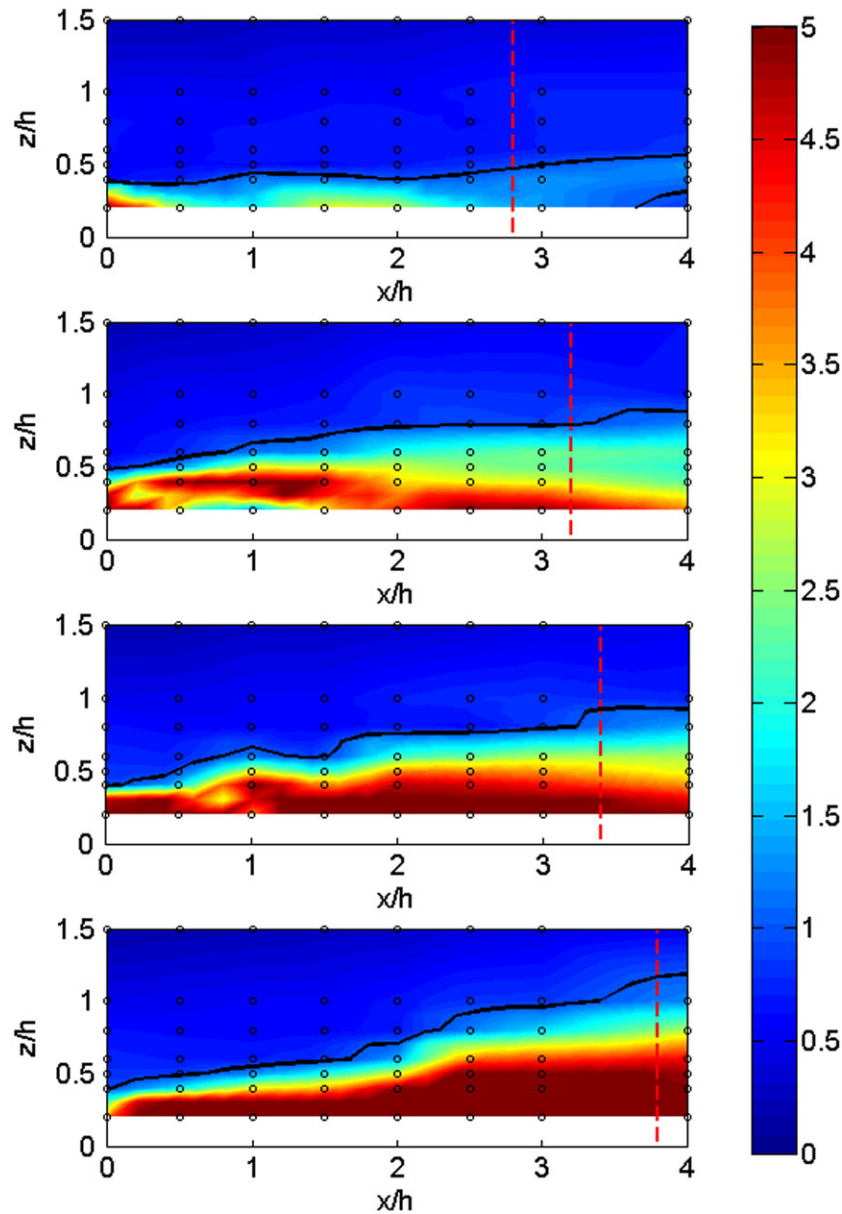


Figure 13. Magnification of normalized cross-covariances in the region immediately downstream of the crest, from $0 < x < 4h$ and $0 < z < 1.5h$.

between the two Cobra Probes relative to the free-stream flow. This increase in correlation persists through the last plane of measurement downstream in each case. The persistent increase in correlation downstream of the separation bubble demonstrates the presence of fluid structures that emanate from the bubble. This is consistent with the structure described by Kiyama and Sasaki.⁴ The presence of these vortex structures causes TI ratio to increase and speed-up to reduce in the downstream region.

Increased yaw angle implies that the probe spacing in the y direction is reduced. Consequently, as the yaw angle was increased, increases in the size of the regions of correlated flow, and increases in the magnitudes of the correlations, were observed. At $\theta = 0^\circ$, the cross-covariance values decay rapidly from the high correlations associated with the separation region, although increased levels of correlation persisted through the farthest downstream plane. By $\theta = 20^\circ$, the reattachment length increased from the $\theta = 0^\circ$ case, and the regions of increased cross-covariance are clearly visible in the $\theta = 20^\circ$ case around the mean reattachment line. From $\theta = 20^\circ$, the size of the correlation region remains almost constant, as evidenced by the cross-covariance = 1 contour presented in each of the plots in Figure 12. However, the magnitude of the correlation continued to increase.

Whilst these experiments have been conducted on flat, smooth surfaces, increased roughness and the presence of obstacles such as fences or vegetation that might be encountered in the field would promote mixing, and thus accelerate the breakdown of the recirculation region and the persistent vortices that propagate downstream.

The development of Strouhal number (St) is presented in Figure 14. The Strouhal number was calculated based on the free-stream velocity, the step height and the highest energy containing frequency from the Power Spectral Density (PSD) of the U -component of the time series at each point. In the low-energy regions, for example, in the undisturbed boundary layer, acoustic peaks were recorded by the Cobra Probes at Strouhal numbers between 0.3 and 0.32. Thus, in the plots presented in Figure 14, where these spikes were evident, the maximum Strouhal number was set to zero.

The colour plots in Figure 14 are scaled to capture Strouhal numbers in the range 0 to 0.5, identifying the shedding from the separation bubble. The Cobra Probes are able to capture fluctuations of frequencies up to the Nyquist frequency of 1250 Hz ($St=1.82$). The maximum Strouhal numbers in the colour plots has been limited to 0.5 because of the ambiguity between the shear layer vortices, the decay of the shear layer vortices to fine-scale turbulence and signal aliasing at the high frequency end of the spectrum. Regions where velocity fluctuations occur at Strouhal numbers greater than 0.5, associated with the shear layer vortices and fine-scale turbulence, are highlighted by the $St=1$ contour. The regions affected by these flow regimes extend between 1 and $1.5h$ vertically from the crest of the step and from the crest to beyond the mean reattachment line.

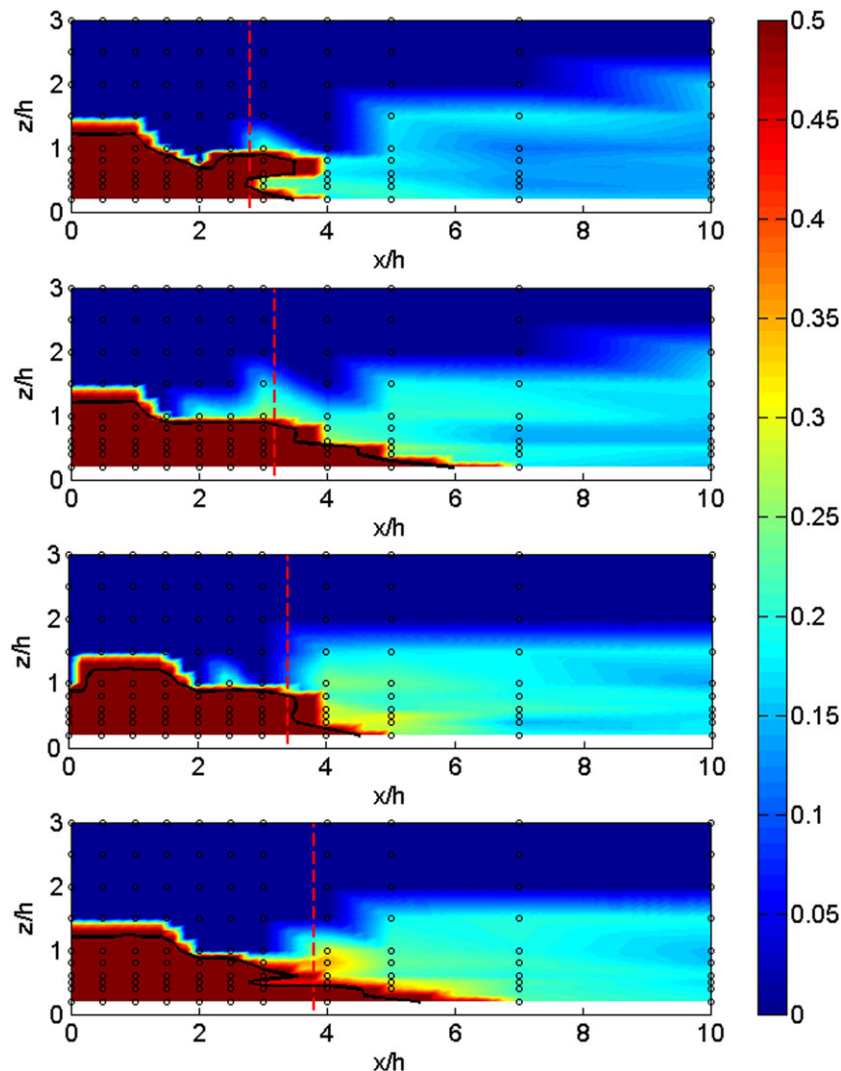


Figure 14. Development of Strouhal number. From top to bottom, yaw angles are 0° , 20° , 30° and 40° . Black circles represent measurement locations. Dashed line is the mean reattachment line. Solid trace represents the $St=1$ contour.

The low-frequency shedding from the recirculation region is present for each of the wind directions examined, illustrated in Figure 14. The peak Strouhal number in the downstream region is in the range 0.15–0.25, independent of yaw angle. This range is consistent with the work of Camussi *et al.*²³

The visualizations of the peak Strouhal numbers in Figure 14 show that there is a decrease in Strouhal number with distance downstream, which implies that the speed at which the vortices propagate downstream reduces with distance downstream, relative to the free-stream velocity. As the yaw angle is increased, the decrease in Strouhal number and thus the decay in vortex propagation velocity are delayed. This is consistent with the increasing stability in the vortex structure induced by the yaw angle.

6. CONCLUSIONS

This work described the effect of yaw angle on flow over an FFS. Velocity measurements provided specific insight into optimal wind turbine siting locations for generic cliff geometry, as well as providing an opportunity to test Baker's hypothesis. The following statistics were considered through a range of inflow yaw angles: speed-up, turbulence intensity, pitch and yaw angles and the identification of vortices shedding from the recirculation region at the crest of the FFS.

Outside of the recirculation region, Baker's hypothesis was shown to be a good approximation to determine the speed-up as a function of yaw angle. Baker's hypothesis can be readily applied as a large number of studies have reported speed-up or velocity measurements for the $\theta=0^\circ$ FFS cases.^{1,5,8,9,26} Discrepancies observed outside of the recirculation and wake regions were of the order of 5%.

Large pitch angles were observed at the crest of the cliff. These were outside the design envelope specified in the standard IEC61400-1.²⁵

Wind turbine rotors will encounter high veer, high TI, lower wind speeds and unfavourable shear profiles should they pass through the recirculation bubble—between the crest and three to four step heights downstream, up to heights of $0.5h$.

Beyond $10h$ downstream of the crest, a wake profile still exists. As the vortices propagate downstream, their gradual diffusion results in an increase in diameter of the vortex. If sited in this region, rotors will be subjected to reduced wind speeds, increased turbulence intensity, wind veer and low-frequency buffeting, all resulting from the vortex ejections from the recirculation bubble. These effects were observed as far downstream as $10h$ and $1.5h$ above the surface of the FFS. The Strouhal number of the buffeting was measured in the range of 0.15–0.25 and was found to be independent of the yaw angle.

A region approximately $0.5h$ downstream of the crest, and above $0.5h$ above the surface, provides a region with the following characteristics: increased wind speed; lowest turbulence intensity at that height and reducing with increased height; pitch angles within the design envelope defined by the standard IEC61400-1²⁵; low wind veer and away from the low-frequency buffeting associated with shedding vortices. This location maximizes energy output, whilst minimizing fatigue loading across the inflow conditions investigated. Shear layer vortices will still be observed in this region.

This work did not consider the lateral variations along the crest of the FFS, which might be encountered due to the inherent ruggedness of cliffs, and is the subject of future research.

ACKNOWLEDGEMENT

This research was supported under the Australian Research Council's Linkage Project funding scheme, project number LP100100746. The authors wish to acknowledge the support of industry partner Entura. Parts of this manuscript were first presented in the conference proceedings of the 16th Australasian Wind Engineering Society Workshop held in Brisbane, Australia, in July 2013 entitled 'Optimal Placement of Wind Turbines on Cliffs'.

REFERENCES

1. Bowen AJ, Lindley D. A wind tunnel investigation of the wind speed and turbulence characteristics close to the ground over various shaped escarpments. *Boundary Layer Meteorology* 1977; **12**: 259–271. DOI: 10.1007/BF00121466.
2. Burton T, Sharpe D, Jenkins N, Bossanyi E. *Wind Energy Handbook*. John Wiley & Sons: Chichester, 2001; 642.
3. Castro IP, Dianat M. Surface flow patterns on rectangular bodies in thick boundary layers. *Journal of Wind Engineering and Industrial Aerodynamics* 1983; **11**: 107–119. DOI: 10.1016/0167-6105(83)90093-4.
4. Kiya M, Sasaki K. Structure of a turbulent separation bubble. *Journal of Fluid Mechanics* 1983; **137**: 83–113. DOI: 10.1017/S002211208300230X.

5. Largeau JF, Moriniere V. Wall pressure fluctuations and topology in separated flows over a forward-facing step. *Experiments in Fluids* 2007; **42**: 21–40. DOI: 10.1007/s00348-006-0215-9.
6. Leclercq D, Jacob M, Louisot A, Talotte C. Forward-backward facing step pair: aerodynamic flow, wall pressure and acoustic characterisation. In *7th AIAA/CEAS Aeroacoustics Conference and Exhibit*. AIAA: Maastricht, The Netherlands, 2001; 075113-1–075113-13.
7. Moss W, Baker S. Re-circulating flows associated with two-dimensional steps. *Aeronautical Quarterly* 1980; **31**: 151–172.
8. Ren H, Wu Y-T. Turbulent boundary layers over smooth and rough forward-facing steps. *Physics of Fluids* 2011; **23**: 1–17. DOI: 10.1063/1.3576911.
9. Sherry M, Lo Jacono D, Sheridan J. An experimental investigation of the recirculation zone formed downstream of a forward facing step. *Journal of Wind Engineering and Industrial Aerodynamics* 2010; **98**: 888–894. DOI: 10.1016/j.jweia.2010.09.003.
10. Hillier R, Cherry NJ. The effects of stream turbulence on separation bubbles. *Journal of Wind Engineering and Industrial Aerodynamics* 1981; **8**: 49–58. DOI: 10.1016/0167-6105(81)90007-6.
11. Kiya M, Sasaki K. Free-stream turbulence effects on a separation bubble. *Journal of Wind Engineering and Industrial Aerodynamics* 1983; **14**: 375–386. DOI: 10.1016/0167-6105(83)90039-9.
12. Saathoff PJ, Melbourne WH. Effects of free-stream turbulence on surface pressure fluctuations in a separation bubble. *Journal of Fluid Mechanics* 1996; **337**: 1–24. DOI: 10.1017/S0022112096004594.
13. Mann J, Angelou N, Sjöholm M, Mikkelsen T, Hansen KH, Cavar D, Berg J. Laser scanning of a recirculation zone on the Bolund escarpment. In *The Science of Making Torque from Wind*. IOP Publishing: Oldenburg, 2012.
14. Ishihara T. Measurements and predictions of local wind field in complex terrain. *Journal of Wind Engineering* 2001; **89**: 245–248.
15. Rowcroft J, Burton D, Blackburn HM, Sheridan J. Surface flow visualisation over forward facing steps with varying yaw angle. *Journal of Physics: Conference Series* 2014; **555**: 012086. DOI: 10.1088/1742-6596/555/1/012086.
16. Baker CJ. The determination of topographical exposure factors for railway embankments. *Journal of Wind Engineering and Industrial Aerodynamics* 1985; **21**: 89–99. DOI: 10.1016/0167-6105(85)90035-2.
17. de Brederode V, Bradshaw P. Three-dimensional flow in nominally two-dimensional separation bubbles: flow behind a rearward-facing step. In *I.C. Aero Report*. Imperial College of Science and Technology: London, 1972; 100.
18. Rowcroft J, Burton D, Blackburn HM, Sheridan J. Surface flow visualisation over forward facing steps with varying yaw angle. In *The Science of Making Torque from the Wind*. Barth S (ed.). IOP: Oldenburg, Germany, 2012.
19. Holmes JD. The atmospheric boundary layer and wind turbulence. In *Wind Loading of Structures*. Taylor & Francis Ltd: London, UK, 2001.
20. Hooper JD, Musgrove AR. Multi-hole pressure probes for the determination of the total velocity vector in turbulent single-phase flow. In *4th International Symposium on Transport Phenomena in Heat and Mass Transfer*. Pacific Centre of Thermal-Fluids Engineering: Sydney, NSW, 1991; 1364–1373.
21. Hooper JD, Musgrove AR. Reynolds stress, mean velocity, and dynamic static pressure measurement by a four-hole pressure probe. *Experimental Thermal and Fluid Science* 1997; **15**: 375–383. DOI: 10.1016/S0894-1777(97)00005-8.
22. Musgrove AR, Hooper JD. Pressure probe measurement of the turbulent stress distribution in a swirling jet. in *Third World Conference on Experimental Heat Transfer, Fluid Mechanics and Thermodynamics*, Kelleher MD, *et al.* (eds). AIP: Hawaii, 1993; 172–179.
23. Camussi R, Felli M, Pereira F, Aloisio G, Di Marco A. Statistical properties of wall pressure fluctuations over a forward facing step. *Physics of Fluids* 2008; **20**. DOI: 10.1063/1.2959172.
24. Lubitz WD, White BR. Wind-tunnel and field investigation of the effect of local wind direction on speed-up over hills. *Journal of Wind Engineering and Industrial Aerodynamics* 2007; **95**: 639–661. DOI: 10.1016/j.jweia.2006.09.001.
25. IEC. IEC 61400 wind turbines. In *Part 1: Design Requirements*. International Electrotechnical Commission: Geneva, 2005.
26. Cochard S, Letchford CW, Earl TA, Montlaur A. Formation of tip-vortices on triangular prismatic-shaped cliffs Part 1: A wind tunnel study. *Journal of Wind Engineering and Industrial Aerodynamics* 2012; **109**: 9–20. DOI: 10.1016/j.jweia.2012.06.003.